Molecular Orientation of Aqueous Surfactants on a Hydrophobic Solid

P. D. BISIO, J. G. CARTLEDGE, W. H. KEESOM, AND C. J. RADKE

Chemical Engineering Department, University of California, Berkeley, California 94720

Received December 14, 1979; accepted February 27, 1980

Direct evidence is presented for the molecular configuration as a function of concentration for aqueous anionic, cationic, and nonionic surfactants adsorbed on a polycarbonate membrane. The polycarbonate surface consists of ionizable weak-acid groups with an average pK value of approximately 4. Hydrodynamic thicknesses, determined from filter viscometry, in conjunction with contact angle and streaming potential measurements, elucidate the adsorption mechanisms. At neutral pH, nonionic and counterion surfactant adsorption occurs in three regions. In the low-concentration Region I, the surfactants lie prone to the surface. Near the CMC, Region II, the surfactants stand vertical with their hydrophobic moiety exposed to the aqueous solution. Very slightly beyond the CMC, Region III commences with tail–tail bilayer adsorption. Co-ion surfactant adsorption does occur, but only in Region I.

INTRODUCTION

Surfactant adsorption at solid boundaries is important in diverse applications such as flotation, detergency, filtration, and oil recovery. In all of these applications it is important to ascertain the configuration of surfactant molecules at the surface. For example, in mineral recovery by air flotation, efficient performance can be anticipated when the surfactant collector adsorbs densely with its hydrocarbon tail oriented away from the surface, rendering the mineral particles more oleophilic. The usual method for studying surfactant adsorption is to contact a solution and a solid, and determine the equilibrium loading from the change in solution concentration. Conjecture about the sorbed configuration is attempted using information on surfactant size and on the surface area of the solid. Such a procedure is not conclusive because of possible patch adsorption, precipitation onto the solid, mixed orientation and multilayers, and ambiguity of the solid surface area appropriate to the size of the adsorbing surfactant.

This work ascertains the structure of anionic, cationic, and nonionic surfactants adsorbed at a negatively charged polycarbonate surface through simultaneous measurement of hydrodynamic layer thicknesses, streaming potentials, and air/water contact angles. The key measurement is that of a hydrodynamic adsorption thickness obtained from filter viscometry. Porous media flow studies have been used extensively in the past to gain valuable information about the structure of polymers adsorbed at the solid–liquid boundary (1–3). However, two difficulties arise when using porous media to divulge surfactant layer thicknesses. First, because surfactant molecules are much smaller in size, finer porous media must be used, and flow data must be more precisely measured. Second, treating a porous medium as a bundle of capillaries with a uniform hydraulic radius is suspect, and clouds interpretation of adsorption thicknesses. We overcome these difficulties by utilizing track-etched polymeric membranes, which resemble quite closely a bundle of uniform cylindrical tubes (4). An

0021-9797/80/110225-10$02.00/0

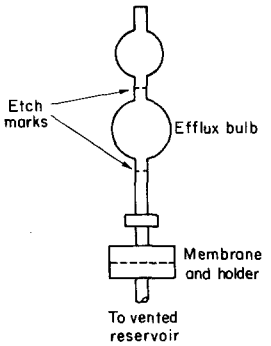

FIG. 1. Filter viscometer.

additional important advantage of the track-etched membranes is that the effect of pore radius can be investigated systematically. The membrane flow studies, when augmented by independent wettability and electrokinetic information, permit deduction of the actual molecular orientation of the adsorbed surfactants as a function of solution concentration.

EXPERIMENTAL

Chemicals

Three surfactants are used in this study: anionic sodium dodecylsulfate (SDS), cationic dodecyltriammonium bromide (DTAB), and nonyloxyethylene octylphenol (Triton X-102). The ionic surfactants are supplied by Eastman Chemical, and the nonionic surfactant by Rohm and Haas. All are used as received from the supplier. However, surface tension measurements with a Rosano tensiometer by the Wilhelmy plate technique reveal only small amounts of impurities. The surface tension data are also used to determine the critical micelle concentrations (CMC) of the surfactants. The indifferent electrolytes are sodium and potassium chloride manufactured by Mallinckrodt as analytical reagent grade. Water is distilled in a Barnstead still, and further purified in a Milli-Q filter system to yield electrical conductivities better than 8×10^{-7} S/cm.

Membranes

Thin (~11 μm) track-etched polycarbonate membranes with pore diameters of 0.6 and 1.0 μm are studied. They are supplied by the Nuclepore Corporation (Pleasanton, Calif.). Scanning electron microscope examination reveals that the pores are not strictly uniform, parallel, cylindrical singlets. Rather some doublets are found, some pores are slightly oblique from the normal, and some pore tapering is present (4). These deficiencies prove minor for interpreting the experiments in this work. From scanning electron photomicrographs we find the mean pore size to be approximately 90% of the nominal value (4, 5).

Filter Viscometry

Flow of dilute surfactants through the Nuclepore membranes is examined in a modified Cannon–Fenske viscometer, as shown in Fig. 1 (6). A 16-cm^3 efflux bulb is attached to a 25-mm Millipore filter holder, which in turn is soldered to a vented beaker permitting immersion in a water bath thermostated at 25 ± 0.1°C. To obtain reproducible results with the filter viscometer requires considerable care in prefiltering and degassing of the solutions. Prefilters of 0.2-μm glass–asbestos and of 0.45-μm cellulose (Millipore) are used in series. Without the second cellulosic prefilter, the glass–asbestos pad, when contacted with the ionic surfactant solutions, fouls the Nuclepore membrane with dislodged fibers. Measurement of the surface tension of the solution before and after filtration demonstrates negligible leaching of impurities from the filters.

For the low Reynolds numbers of the flow experiments (i.e., $<10^{-3}$), and for small differences in calibration and surfactant solution efflux times, calculated entrance and exit losses through the membrane pores are small (6, 7). Likewise, any surface tension correction is unimportant (6, 8).

Nevertheless, it is paramount to establish that the filter apparatus behaves as a conventional viscometer. We determine the viscosity of 0.1 N sodium chloride solutions in the filter viscometer and in a standard Cannon–Fenske capillary viscometer at three temperatures. Saline solutions are used to eliminate electroretardation, which is readily detected by the filter viscometer (6). Figure 2 gives the ratio of the apparent viscosity in the filter viscometer and the bulk viscosity in the capillary viscometry, μ_a/μ, as a function of temperature, divided by that same ratio at the arbitrary reference temperature, T_0. For valid viscometry, this quantity should be unity. Over the 20% range of kinematic viscosity, μ/ρ, encompassing the surfactant flow studies, Fig. 2 demonstrates that the filter apparatus does indeed measure fluid viscosity. The slight deviation from unity, which is within experimental error, can be rationalized in terms of small kinetic energy losses at the pore entrances and exits (6, 7, 9).

When measuring surfactant solution viscosities against the saline calibrating fluid, we find a steady efflux after one bulb volume of surfactant solution. Because only time and volume are measured, the filter viscometer gives precise results, as seen from the maximum observed error bars in Fig. 2. Further details of the viscometry experiments are available in Ref. (6).

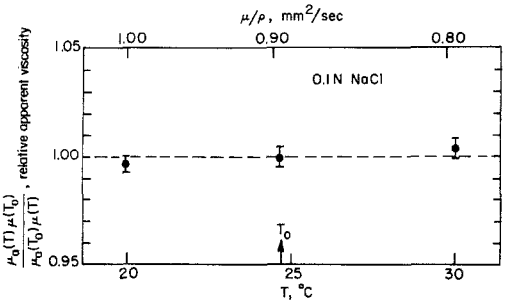

FIG. 2. The relative apparent viscosity ratio of salt water in the filter viscometer and in a capillary viscometer as a function of temperature, and kinematic viscosity, μ/ρ.

Contact Angles

Contact angles are measured on a Ramé–Hart goniometer with a covered quartz–stainless-steel cell. The membranes are clamped with their rough face against glass slides by a Teflon holder. Considerable care is taken to align the membrane both along and transverse to the goniometer axis. The water-advancing angle is 65°, whereas the water-receding angle is 28°. These values are almost identical to those measured against silver iodide, which is traditionally considered a hydrophobic surface (10, 11). For this reason, and because the membranes are bulk polycarbonate, we classify the Nuclepore surface as hydrophobic.

For the surfactant solution angles, an air bubble is slowly formed and allowed to rise a short distance through the solution, and contact the membrane. Therefore, we are reporting water-receding angles although, when measured in this fashion, such contact angles are sometimes called equilibrium angles (12). After equilibration for about 90 min, contact angles are measured on both sides of a large number of air bubbles interspersed across the membrane, and the average noted. We can reproduce contact angles to within ±2°, which is consistent with other researchers (10, 11, 13, 14). Because the membranes are riddled with pores, there is some concern that pore edges may affect the contact angles (15). However, the pores are very small compared to the air bubbles, and we are mainly interested in the relative changes of contact angles upon surfactant adsorption.

Streaming Potentials

A schematic of the streaming potential apparatus is shown in Fig. 3. A pulse-dampened constant-rate pump (FMI) supplies closed-loop flow through the 47-mm Nuclepore membrane, housed in a Plexiglas cell, into a reservoir blanketed by humidified

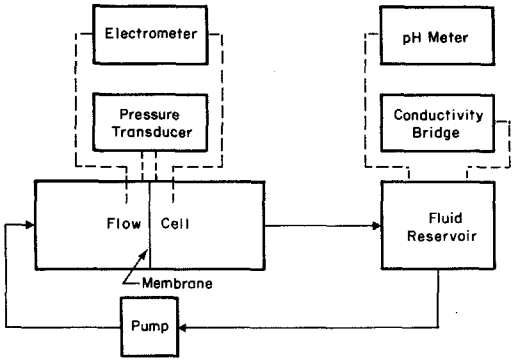

FIG. 3. Schematic of the streaming potential apparatus.

nitrogen. This closed-loop design provides stability against electrical interference, and permits measurement of small ζ potentials. The flowing solutions come into contact only with Plexiglas, nylon, Teflon, and glass. A Validyne reluctance transducer monitors the pressure drop, and the generated electrical potential is measured by reversible silver–silver chloride electrodes, prepared according to Gray (16), and a Kiethley electrometer. Because of the high impedance of the electrometer, measured potential differences are independent of the distance between the detecting electrodes. We find the silver–silver chloride electrodes to be stable with little or no offset potentials, thus circumventing many of the experimental difficulties reported by Ball and Fuerstenau (17). Two plastic screens provide mechanical support for the membrane, and "O"-ring seals prevent leakage around the membrane. Since the pressure drop across the support screens is small compared to that across the membrane, the screens do not contribute to the overall streaming potential. Conductivity and pH are measured in the reservoir in the usual manner.

The pressure drop and electrical potential difference across the membrane are recorded for a number of increasing and decreasing flow rates and directions. ζ potentials are then calculated from the best-fit slope of the straight line between potential and pressure drop, and the Smoluchowski equation, with the measured bulk conductivity, and the viscosity and permittivity of pure water at ambient temperature (i.e., 22°C). More information on the experimental apparatus and procedures is available elsewhere (18).

To characterize the surface of the track-etched polycarbonate membrane, the ζ potential is reported in Fig. 4 as a function of pH at constant ionic strength. The membrane exhibits a slight negative surface charge, which increases in magnitude with increasing pH. Below a pH of 3 the surface is neutral, and above a pH of about 6 the surface is fully charged. All the surfactant experiments to follow are performed at neutral pH, and it is important to remember that the membrane surface is negatively charged.

The solid line in Fig. 4 corresponds to a theoretical model which assumes that the polycarbonate surface consists of one type of ionogenic weak-acid group (18, 19). This model predicts that the surface groups have a pK of about 4 and a surface number density of 10^{16} groups/m^2 (i.e., a surface charge density of 0.2 μC/cm^2 when fully ionized). This number density indicates one ionogenic group for every 8000 Å^2, and reflects a sparsely charged surface. The maximum observed error bars in Fig. 4 are

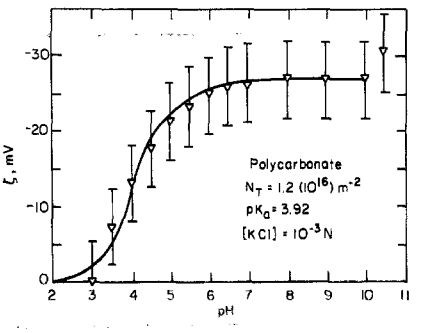

FIG. 4. The ζ potential of polycarbonate membranes as a function of pH in 10^{-3} N potassium chloride. The solid line is fit to an ionogenic surface group model with a maximum charge density of 1.2×10^{16} groups/m^2, and a pK_a of 3.92 (18, 19).

due mainly to variability among different membranes.

RESULTS AND DISCUSSION

Filter Viscometry

Results for the steady-state apparent viscosity of DTAB solutions relative to the bulk viscosity are shown in Fig. 5 for two different mean pore diameters. Since the surfactant solutions in this study are all dilute, the bulk viscosity is equivalent to the calibrating salt solution. The apparent viscosities in Fig. 5 are reversible in the sense that identical values are found either by increasing or by decreasing the solution concentration. No effect is found until near the CMC of DTAB where a steep rise is evident. A maximum value is reached just beyond the CMC that is unchanged by further increases in concentration. Note that the apparent viscosity is larger the smaller the pore diameter.

One explanation for the results in Fig. 5 is presence of micellar structures slowing flow in small pores. This explanation, however, is untenable because the concentration of micelles increases dramatically above the CMC, whereas Fig. 5 shows no additional increase in apparent viscosity in this region. SEM photographs do not reveal particulate matter on the membrane. Hence, a likely possibility is constriction

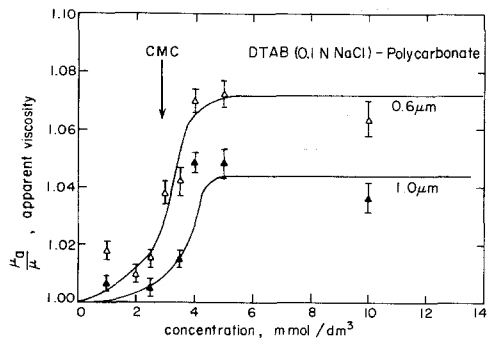

FIG. 5. The apparent viscosity of saline DTAB solutions in 0.6- and 1.0-μm-pore-diameter polycarbonate membranes.

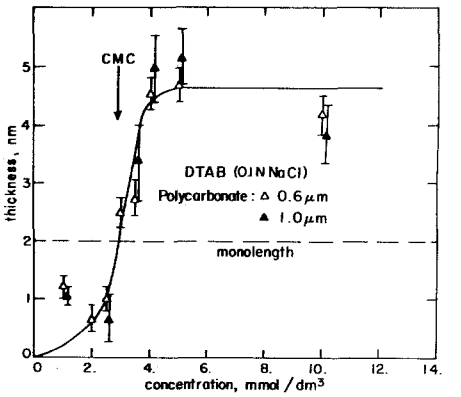

FIG. 6. The adsorption thickness for saline DTAB solutions in 0.6- and 1.0-μm-pore-diameter polycarbonate membranes. The dashed line indicates the length of the surfactant molecule.

of flow due to adsorbed layers on the pore walls. To test this hypothesis, we assume that the viscosity of the adsorbed surfactant layer is sufficiently large (i.e., approaching infinity) so that no-slip may be imposed at the adsorbed-layer solution interface. Then, the Hagen–Poiseuille expression is applicable for calculating layer thicknesses (i.e., thickness $= r_0[1 - (\mu/\mu_a)^{1/4}]$, where r_0 is the pore radius). Because the Hagen–Poiseuille analysis specifies a fourth root of the apparent viscosity data, meaningful layer thicknesses may be determined.

Figure 6 gives the calculated thicknesses for DTAB from Fig. 5. For the adsorbed layer model to be correct the thickness must be independent of the pore diameter. Figure 6 confirms this, and provides strong evidence for the layering hypothesis. The dashed line in Fig. 6 indicates the length of the DTAB molecule calculated from individual bond lengths (6). Additional apparent viscosity data, not shown in Figs. 5 and 6 (and in Fig. 7 to follow) for concentrations decades lower than and up to the CMC, show no adsorption thicknesses. Thus, we speculate that below the CMC, DTAB molecules do not adsorb or they adsorb in a non-flow-restricting manner. Near the CMC vertical adsorp-

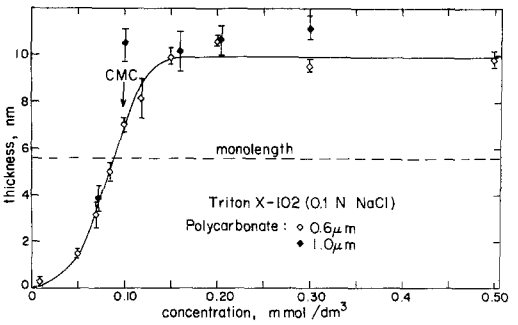

FIG. 7. The adsorption thickness for saline Triton solutions in 0.6- and 1.0-μm-pore-diameter polycarbonate membranes. The dashed line indicates the length of the surfactant molecule.

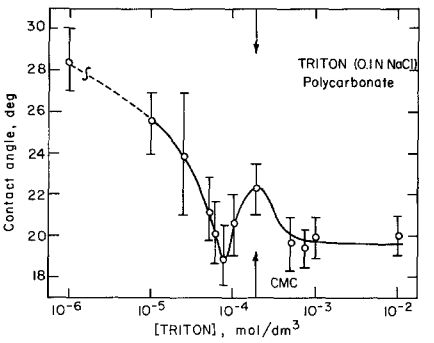

FIG. 9. Air receding-water contact angles for saline Triton solutions on polycarbonate membranes.

tion occurs, and above the CMC a bilayer forms.

Since the measured quantity in these experiments is a resistance to flow rather than a direct measure of adsorption, patchwise adsorption remains a possibility. However, such patch-adsorption regions must be sufficiently close together for the flowing solution to see complete coverage. The steep rise in thickness near the CMC suggests that uniform filling in of bilayer patches formed at much lower concentration is not occurring; likewise, filling in of vertically oriented monolayer patches is rejected.

Figure 7 gives the thickness results for the nonionic surfactant, Triton, in 0.6- and 1.0-μm pores. The results are almost identical to those for DTAB, except that the adsorption thickness is larger, because the Triton molecule is longer, and the concentrations are an order of magnitude lower. The concentrations at which flow reduction occurs are lower because the CMC of Triton is almost a decade lower. However, for SDS, which is of the same charge as the membrane surface, the apparent viscosity is unity over the entire concentration range. This suggests that vertical and bilayer adsorption do not occur for co-ion surfactants.

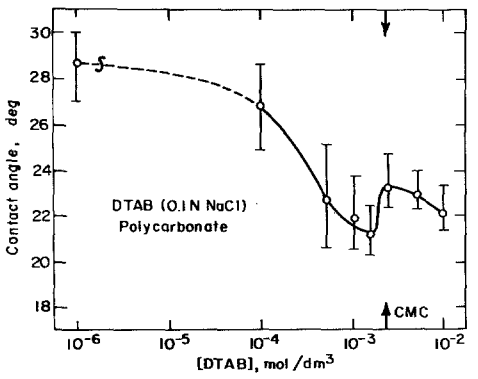

FIG. 8. Air receding-water contact angles for saline DTAB solutions on polycarbonate membranes.

Contact Angles

Air water-receding contact angles are reported in Figs. 8 through 10 for the three surfactants. Below the CMC, all surfactants show a decreasing contact angle with increasing concentration. As the surface tension of these solutions falls by about 60% in the concentration region up to the CMC (6, 18), Young's equation dictates a decreasing adhesion tension (10, 20). Consequently, in spite of no observed flow retardation until the CMC is reached, adsorption of the surfactants at the solid surface is taking place to make the membrane more hydrophobic.

Near the CMC, the contact angles of both DTAB and Triton increase to a maximum, and then decrease just beyond the CMC.

Although the receding angle changes are small, the maxima are always reproduced each time the experiment is repeated. Again, Young's equation, applied to the concentration region of increasing contact angle, indicates a further increase in hydrophobicity of the membrane surface. Above the CMC, the surface tension levels off so the decrease in contact angles for DTAB and Triton designates an increasingly hydrophilic membrane surface. Since the contact angles exhibit abrupt variations at the same concentrations as observed for the abrupt variations of hydrodynamic thickness in Figs. 6 and 7, we conclude that both experiments reflect the identical adsorption phenomena at the polycarbonate surface. We further conclude that the properties of the membrane surface are similar in the pores and on the external faces.

It is fascinating that Fig. 10 shows no maximum contact angle for SDS. Rather the adhesion tension decreases monotonically until the CMC, and then becomes constant. Apparently, the surfactant adsorption mechanism which causes the hydrodynamic thickness increase and the contact angle maximum is not operative for the co-ion surfactant, SDS.

Streaming Potentials

Figure 11 gives the ζ potentials, calculated from the measured streaming potentials, for the three surfactants in a background of 10^{-3} N potassium chloride. The positive counterion DTAB adsorbs strongly and reverses the net membrane surface charge at a concentration considerably below the CMC. Because no flow restriction is found at these concentrations, the origin of the charge reversal is not hemimicellization (21–23). Likewise, the decrease in ζ potential for Triton indicates adsorption below the CMC. Most importantly, the slight increase in the negative ζ potential of the membrane with SDS confirms co-ion adsorption. This agrees with the contact angle findings in Fig. 10. Kayes (24) also reports an increased negative ζ potential for SDS adsorbing onto anionic polystyrene latices.

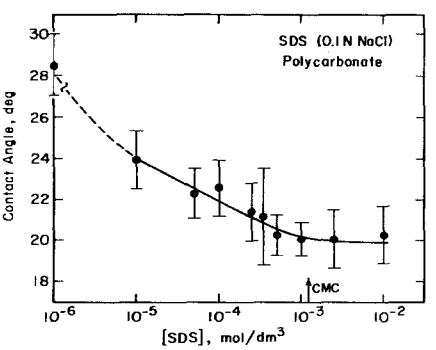

FIG. 10. Air receding-water contact angles for saline SDS solutions on polycarbonate membranes.

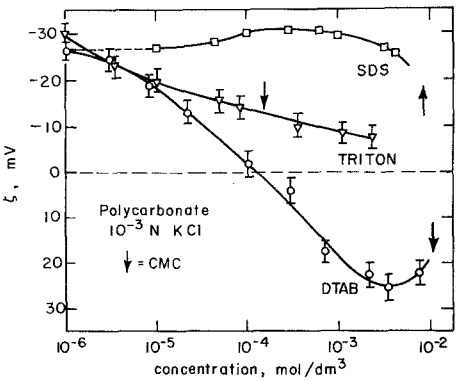

FIG. 11. ζ potentials for SDS, Triton, and DTAB solutions adsorbed on polycarbonate in 10^{-3} N KCl.

Adsorption Orientation

Thickness, contact angle, and ζ potential results are compared in Figs. 12 and 13 for the counterion surfactant, DTAB, and the nonionic surfactant, Triton, respectively. To obtain a consistent explanation for all the data, these figures may be divided into three concentration regions: Region I below the CMC, Region II near the CMC, and Region III above the CMC. In Region I no adsorption thickness is found, but the contact angles and ζ potentials reveal adsorption to increase the membrane hydro-

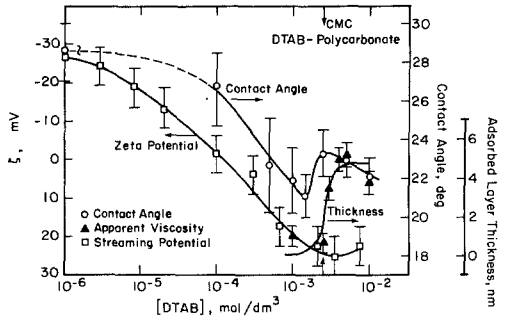

FIG. 12. Comparison of contact angles, ζ potentials, and adsorption thicknesses for DTAB on polycarbonate membranes. ζ potentials are in 10^{-3} N KCl. All other data are for 0.1 N salt.

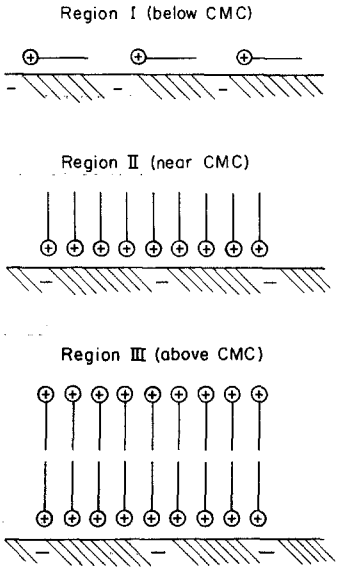

FIG. 14. Schematic of adsorption configurations for DTAB and Triton on the anionic polycarbonate surface. SDS adsorbs according to Region I only.

phobicity. Hence, the adsorption orientation is horizontal to the surface, as depicted in Fig. 14. Presumably, surfactant adsorption is controlled by van der Waals and entropy-driven hydrophobic-bonding forces between the hydrocarbon tail and the polymeric surface, and, in the case of the cationic surfactant, is augmented by electrostatic attraction. Slightly below the CMC, the beginning of Region II, the adsorption thickness builds to approximately the length of the surfactant molecule, and ζ potentials and contact angles show further adsorption, with a transition to increased hydrophobicity. Thus, as seen in Fig. 14, surfactant orientation is vertical to the surface. Apparently, a sufficient adsorption amount is established for lateral tail–tail interactions to dominate. The surfactant molecules may therefore stand up. Just above the CMC, where Region III starts, the adsorption thickness changes to twice the surfactant length, and the contact angles demand a more hydrophilic surface. Hence, according to Fig. 14, adsorption orientation is bilayer. Once the surfactants are oriented vertical with their tails exposed to the aqueous solution, the same hydrophobic-bonding forces responsible for micellization quickly complete the second layer. Electrostatic and solvation forces prevent the buildup of additional layers. Both the cationic surfactant and the nonionic surfactant behave identically, except for the differences in their CMC values. The adsorption sequence outlined here is essentially that deduced by Billett and Ottewill (10) for dodecylpyridinium bromide on an ionic silver iodide surface. However, we do not find a mixed orientation state where the fraction of surfactant molecules standing up

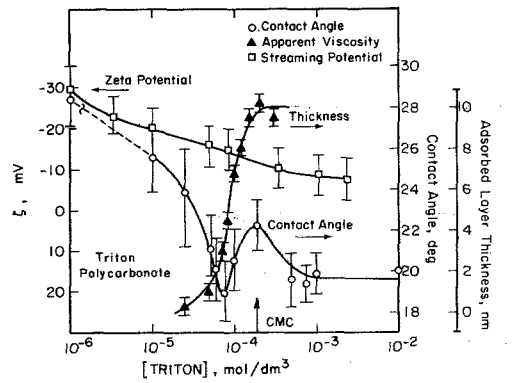

FIG. 13. Comparison of contact angles, ζ potentials, and adsorption thicknesses for Triton on polycarbonate membranes. ζ potentials are in 10^{-3} N KCl. All other data are for 0.1 N salt.

gradually increases. Here, the transition from planar to vertical configuration is reasonably sharp.

The possibility of bimolecular leaflet formation at a solid–liquid boundary is common in flotation literature (25). It has been inferred from adsorption densities (10, 26–30), contact angles (10, 31), flotation response (10, 29), colloid stability (10, 29), electrokinetics (30), sedimentation volume (28, 32), and retained liquid films (20). Some, early assertions of sorbed bilayers, especially those deduced solely from adsorption density, have been criticized by Sutherland and Wark (25). The present work provides direct evidence that hydrophilic bilayer structures at the solid–aqueous interface do indeed exist. Further, we find no interpenetration of the surfactant hydrocarbon tails in the leaflet, so that the bilayer thickness is essentially twice the length of the surfactant molecule. Lateral tail–tail interactions appear sufficiently strong so that there is little free-energy advantage for significant interdigitation. Studies on black lipid membranes (33), and Langmuir–Blodgett layers (34) confirm this finding.

Figure 15 compares the ζ potentials and contact angles for the co-ion surfactant, SDS. No adsorption thickness is measured for this molecule. Based on our previous arguments, Fig. 15 shows that SDS adsorbs horizontally in Region I only. Vertical orientation, and bilayering do not occur. Because the attractive van der Waals and/or hydrophobic-bonding forces for SDS must overcome an increasing electrostatic repulsion from the anionic membrane surface, adsorption density is less than for DTAB or Triton. Presumably sufficient coverage is not reached for enough tail–tail interactions to promote a head-outward vertical configuration (i.e., a vertical orientation with the co-ion surfactant head group adjacent to the anionic surface is unlikely). All previous studies of bilayer adsorption, in which the charge of the solid substrate is mentioned, indicate bimolecular structures

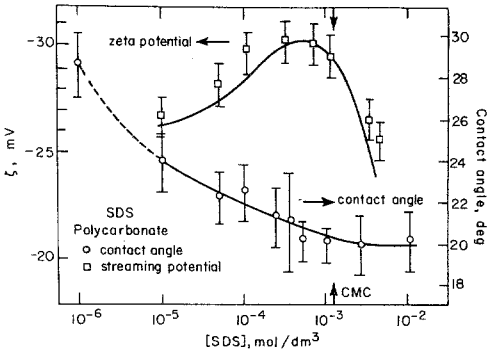

FIG. 15. Comparison of contact angles and ζ potentials for SDS on polycarbonate membranes. No adsorption thickness is found. ζ potentials are in 10^{-3} N KCl. The remaining data are for 0.1 N salt.

only for nonionic surfactants or for ionic surfactants whose charge is opposite to that of the surface (10, 20, 28, 30). Further, these studies show that bilayers form slightly above the surfactant CMC. Figures 12 through 15 consolidate these conclusions.

One uncertainty remains about patchwise adsorption. The low contact angles suggest incomplete filling in of the surface, possibly in the form of adsorption islands. Conversely, as mentioned above, the hydrodynamic thicknesses require such adsorption patches, if they exist, to be located sufficiently close together in order to restrict flow as if the entire surface were covered. Without precise adsorption and membrane surface area measurements, we cannot resolve this question.

CONCLUSIONS

Adsorption of DTAB, Triton, and SDS is studied on hydrophobic polycarbonate membranes track-etched to consist of monodisperse cylindrical pores. From electrokinetic characterization, the membrane surfaces contain a low density of weak-acid groups, which are completely ionized at neutral pH. Concurrent measurements of hydrodynamic adsorption thicknesses, contact angles, and streaming potentials permit elucidation of surfactant adsorption con-

figuration. The counterion and nonionic surfactants orient differently in three concentration regions. In Region I, up to the CMC, adsorption is horizontal to the surface. Just below the CMC, Region II, the molecules stand vertically with their hydrocarbon tails adjacent to the aqueous solution. Slightly above the CMC, where Region III commences, a hydrophilic bilayer forms. Co-ion surfactant adsorption is found, but only in Region I.

ACKNOWLEDGMENTS

Support of the National Science Foundation under Grant ENG76-84159 is acknowledged. This work was presented at the ACS/CSJ Chemical Congress, Honolulu, Hawaii, April 2–6, 1979. P.D.B. is grateful for partial support from the Lawrence Berkeley Laboratory as a summer undergraduate research scholar.

REFERENCES

1. Bulas, R., Rolhstein, E., Rowland, F., and Eirich, F. R., *Ind. Eng. Chem.* **57,** 46 (1965).
2. Rowland, F., and Eirich, F. R., *J. Polymer Sci. Part A-1* **4,** 2033 (1966).
3. Rowland, F., and Eirich, F. R., *J. Polymer Sci. Part A-1* **4,** 2401 (1966).
4. Porter, M. C., *Amer. Lab.* **63,** Nov. (1974).
5. Spurny, K., and Lodge, J. P., Jr., *Collect. Czech. Chem. Commun.* **33,** 3679 (1968).
6. Cartledge, J. S., M.S. thesis, Chemical Engineering Department, Pennsylvania State University, University Park, Pa. (1976).
7. Vrentas, J. S., and Duda, J. L., *Appl. Sci. Res.* **28,** 241 (1973).
8. Cannon, M. R., and Fenske, M. R., *Ind. Eng. Chem.* **10,** 297 (1938).
9. Bingham, E. C., "Fluidity and Plasticity." McGraw–Hill, New York, 1922.
10. Billett, D. F., and Ottewill, R. H., "Wetting," *Soc. Chem. Ind.* **25,** 253 (1967).
11. Osseo-Asare, K., Fuerstenau, D. W., and Ottewill, R. H., *Amer. Chem. Soc. Symp. Ser.* **8,** 63 (1975).
12. Wakamatsu, T., and Fuerstenau, D. W., *Trans. Soc. Min. Eng. AIME* **254,** 123 (1973).
13. Zisman, W. A., and Fox, H. W., *J. Colloid Sci.* **5,** 514 (1950).
14. Yiannos, P. N., *J. Colloid Sci.* **17,** 334 (1962).
15. Oliver, J. F., Huh, C., and Mason, S. G., *J. Colloid Interface Sci.* **59,** 568 (1977).
16. Gray, D. H., Ph.D. thesis, Material Science Department, University of California, Berkeley, Calif. (1966).
17. Ball, B., and Fuerstenau, D. W., *Miner. Sci. Eng.* **5,** 267 (1973).
18. Keesom, W. K., M.S. thesis, Chemical Engineering Department, University of California, Berkeley, Calif. (1977).
19. Keesom, W. K., Zelenka, R. L., and Radke, C. J., presented at the 71st Annual Meeting of AIChE, Miami Beach, Florida, November 13–17, 1978.
20. O'Connor, D. J., and Sanders, J. V., *J. Colloid Sci.* **11,** 158 (1956).
21. Gaudin, A. M., and Fuerstenau, D. W., *Trans. AIME* **202,** 958 (1955).
22. Fuerstenau, D. W., *Pure Appl. Chem.* **24,** 135 (1970).
23. Fuerstenau, D. W., *in* "The Chemistry of Biosurfaces," (M. L. Hair, Ed.), Vol. 1, p. 143. Dekker, New York, 1971.
24. Kayes, J. B., *J. Colloid Interface Sci.* **56,** 426 (1976).
25. Sutherland, K. L., and Wark, I. W., "Principles of Flotation." Aust. Inst. Min. Met., Melbourne, 1955.
26. Held, N. A., and Samochivalov, K. N., *Kolloid Z.* **72,** 13 (1935).
27. Held, N. A., and Khainsky, I. A., *Kolloid Z.* **76,** 26 (1936).
28. Cuming, B. D., and Schulman, J. H., *Aust. J. Chem.* **12,** 413 (1959).
29. Jaycock, M. J., and Ottewill, R. H., *Trans. Inst. Min. Met. (London)* **72,** 497 (1963).
30. Mathai, K. G., and Ottewill, R. H., *Trans. Faraday Soc.* **62,** 750, 759 (1966).
31. Schulman, J. H., and Leja, J., *Trans. Faraday Soc.* **50,** 598 (1954).
32. Moilliet, J. L., and Collie, B., "Surface Activity." Van Nostrand, New York, 1951.
33. Tien, H. T., "Molecular Association in Biological and Related Systems," Adv. Chem. Ser., Vol. 84, p. 104. Amer. Chem. Soc., Washington, D.C., 1968.
34. Gaines, G. L., Jr., "Insoluble Monolayers at Liquid–Gas Interfaces." Interscience, New York, 1966.